ELSEVIER

Solid State Ionics 109 (1998) 259–272

SOLID STATE IONICS

Interfacial studies of solid-state cells based on electrolytes of mixed ionic–electronic conductors

Hongxing Hu, Meilin Liu*

School of Materials Science and Engineering, Georgia Institute of Technology, Atlanta, GA 30332-0245, USA

Received 13 January 1998; accepted 9 February 1998

Abstract

Combination of 4-probe impedance and polarization measurements offers an effective approach to investigate electrode kinetics and transport properties of each cell component in a solid-state electrochemical cell based on an electrolyte of mixed ionic–electronic conductor (MIEC). In particular, two representative solid-state cells, one with an electrolyte of an MIEC ($Pt \mid BaCe_{0.8}Gd_{0.2}O_3 \mid Pt$) and the other with an electrolyte of an ionic conductor ($Pt \mid Bi_{1.5}Y_{0.5}O_3 \mid Pt$), are used as examples to demonstrate the uniqueness of these techniques in separating the response of each cell component, in measuring the interfacial polarization resistance and overpotential of each individual interface, in identifying reaction mechanisms (the nature of rate-limiting steps), and in determining kinetic parameters.

Keywords: Interfaces; Mixed conductors; MIEC; 4-probe measurement; Electrode kinetics

1. Introduction

The operation of a solid-state electrochemical system, in general, involves mass transport through each cell component and various electrochemical processes at the electrode–electrolyte interfaces, including adsorption–desorption, dissociation–association, chemical reactions, charge transfer, and mass transfer. While the resistance of each cell component must be sufficiently low to achieve high performance, the electrochemical processes occurring at the interfaces between cell components play an even more important role in determining the performance of many solid-state electrochemical devices, such as solid oxide fuel cells (SOFCs), gas sensors, and gas separation systems using membranes of mixed ionic–electronic conductors (MIECs). Often, insufficiently-fast interfacial processes are found to be responsible for unsatisfactory device performance [1–13]. For instance, the power output of an SOFC based on thin-film electrolyte is often limited by the polarization loss at the electrode–electrolyte interfaces [5–10]. Similarly, the speed of response of a solid-state gas sensor and the efficiency of a gas separation system based on thin-film MIEC membranes are greatly influenced by the kinetics of interfacial processes [5,6,11–13]. In searching for systems to be operated at low temperatures based on new materials and thin-film structures, the device performance depends more on interfacial properties, because the kinetics of interfacial processes become dominant as the operating temperature is lowered and as the thickness of the electrolyte

*Corresponding author. Tel.: +1 404 894 6114; fax: +1 404 894 9140; e-mail: meilin.liu@mse.gatech.edu

0167-2738/98/$19.00
PII: S0167-2738(98)00095-2

is reduced. The ability to characterize each individual cell component and interface in a solid-state electrochemical system allows direct evaluation of the performances of each component and interface in the system, and hence identification of the rate-limiting factor to overall device performance, providing valuable information for most effective improvement of device performance.

Schematically shown in Fig. 1 are two typical cell configurations used for investigation into the electrochemical behavior of solid-state cells. In some cases, the materials and geometries of the two principal electrodes, the working and counter electrode, are identical, as are the atmospheres to which the two electrodes are exposed. Such a cell is referred to as a symmetrical cell. In some other cases, it is desirable to investigate the response of a cell in-situ when it is subjected to the real service conditions. For instance, the cathode and anode of an SOFC are usually made of different materials and each electrode is exposed to different atmospheres. Such an SOFC, then, is asymmetric. Two techniques have been used to characterize solid-state electrochemical systems: DC polarization measurements [14,15] and AC impedance spectroscopy [15,16]. These techniques, together with multiple (3 or 4) probes [6,17–20], have been successfully used to separate the performance of individual cell component in solid-state electrochemical systems. In all previous studies, however, the cells studied were based on electrolytes of ionic conductors, in which electronic transport has been neglected in analysis. Accordingly, the interpretation

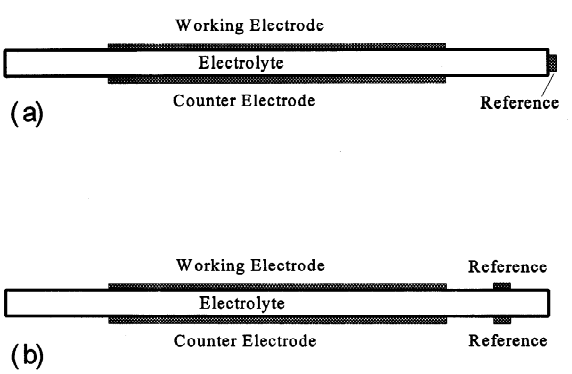

Fig. 1. Schematic views of symmetrical cells with (a) a 3-electrode and (b) a 4-electrode configuration for interfacial studies of solid-state cells.

of impedance spectra and polarization data presented in previous studies does not apply to cells based on electrolytes of MIECs, in which electronic transport is significant. In this paper, the application of multi-probe impedance spectroscopy and DC polarization measurements to studies of interfaces of solid-state electrochemical systems will be elaborated on a broader basis, covering systems based on MIEC electrolytes. The term 'interface' in this paper specifically refers to an electrode–electrolyte interface. On the other hand, the characteristics of an 'electrode' in a solid-state cell depend critically on the properties of the electrode–electrolyte interface, as generally understood. For simplicity, the two terms are used interchangeably in this paper.

2. Experimental methods

2.1. Sample preparation

Both gadolinium-doped barium cerate, $BaCe_{0.8}Gd_{0.2}O_3$ (BCG), and yttria-stabilized bismuth oxide, $Bi_{1.5}Y_{0.5}O_3$ (BY), were used as electrolytes in this study. BCG is an MIEC in oxygen-rich atmospheres [21–25], while BY is a nearly pure oxygen ionic conductor [26,27]. Both materials are promising candidates for intermediate-temperature solid-state electrochemical devices. Pellets of BCG and BY (about 15 mm in diameter and about 1 mm thick) were prepared using a traditional ceramic process [28]. The pellets were polished flat, resulting in a thickness of 0.8–0.9 mm. For simplicity and reproducibility, platinum was used as electrode material throughout this study. Paste of platinum (Heraeus OS2) was screen printed on the electrolyte pellets and subsequently fired using different temperature profiles depending on the electrolyte materials. Samples with BCG electrolyte were fired at temperatures ranging from 1200 to 1400°C for 5 to 30 min, while samples with BY electrolyte were fired at 900°C for 10 min. Modification in processing conditions, such as firing temperature and soaking time, resulted in two types of Pt electrodes. Electrodes fired at lower temperatures and for a shorter period of time were porous, whereas electrodes fired at higher temperatures and for a longer period of time were relatively dense. However, systematical

comparison between the two types of electrodes will not be made, since the objective of this study is to demonstrate the methodology and the application of the measurement techniques rather than to address considerations of materials and processing.

2.2. Cell configuration

As schematically shown in Fig. 1, both 3-electrode and 4-electrode configurations were studied. In both cases, two circular electrodes (working electrode and counter electrode) in a diameter of 7 mm were symmetrically printed at the face centers of the electrolyte pellets [25]. In the case of 3-electrode configuration, a dot of Pt was placed at the side of the pellets as a reference electrode (Fig. 1(a)). In the case of 4-electrode configuration, two reference electrodes in the form of Pt-dot were placed at edges of the two faces of the pellets, about 2 mm away from the principal electrodes (Fig. 1(b)). Silver leads were then attached to the electrodes with silver solder, which was fired at 750°C to ensure good contacts.

To discuss the positioning of the reference electrodes, we must start with a qualitative description of the field and potential distributions in the electrolyte of the testing cell when a voltage is applied to the two principal electrodes. Shown in Fig. 2 is a schematic sketch of such distributions. Because the thickness of the electrolyte is much (in orders of magnitude) smaller than the diameter of the electrodes, the flux of the electric field is mostly confined in the cylindric volume of the electrolyte between the two principal electrodes, while the lines of field are sparsely distributed outside this volume, bending outwards (Fig. 2(a)). This results in a large gradient in electrical potential near the edges of the electrodes (Fig. 2(b)). In the directions away from the electrodes, the electrical potential at the electrolyte surface initially changes dramatically with the distance away from the electrode edges, then quickly approaches the median of the two electrode potentials, which is defined by the equipotential plane coincident with the symmetrical plane of the cell. Numerical analysis showed that, at a distance (away from the electrode) greater than a few times of the thickness of the electrolyte, the electrical potential at the electrolyte surface assumes a value virtually equal to the median of the two electrode potentials. In other words, a reference electrode positioned sufficiently far away from the principal electrodes (a few times of the electrolyte thickness) sees the median of the potentials of the two principal electrodes, or the potential at the symmetrical plane of the cell. This is particularly true in the case of 3-electrode configuration, since the reference electrode is positioned on the side of the pellets, which lies on the symmetrical plane of the cell. In the case of 4-electrode configuration, the two reference electrodes are sufficiently far away from the principal electrodes and thus both of them see the same electrical potential. This was actually confirmed by an experiment: the potential difference of the two reference electrodes is always measured to be zero in the presence of an electrical potential difference between the two principal electrodes when the cell is immersed in a uniform atmosphere.

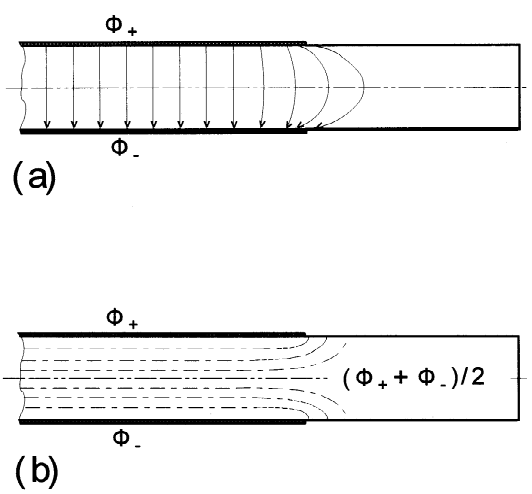

Fig. 2. Schematic distributions of (a) field flux (solid lines) and (b) equipotential planes (dashed lines) in the testing cells shown in Fig. 1 (only half of the cell is shown).

The discussion so far has been based on the assumption that all the electrodes are exposed to a uniform atmosphere. In this case, the 3-electrode and 4-electrode configurations are of minimal difference. The 3-electrode configuration is preferred because of its simplicity. When a chemical potential is imposed to the cell, i.e., one of the principal electrodes is exposed to one atmosphere whereas the other is exposed to a different atmosphere, as in the case of

some real devices such as an SOFC, the above discussion about the distribution of 'electrical' potential still holds (because of the additive nature of the electrical and chemical potential). However, the observable (or measurable) potential difference between the two reference probes in a 4-electrode configuration is no longer zero, but equal to the chemical potential difference of the two reference electrodes (or the two atmospheres). This is because, in general, the measurable voltage across the two reference electrodes (re1 and re2), $V_{re1-re2}$, can be expressed as

$$V_{re1-re2} = \frac{1}{F}[(\mu_{re1} - F\Phi_{re1}) - (\mu_{re2} - F\Phi_{re2})] \quad (1)$$

where μ_{re1} and μ_{re2} are the chemical potential of electrons at the surface of the MIEC electrolyte in contact with re1 and re2, respectively, whereas Φ_{re1} and Φ_{re2} are the electrical potential of re1 and re2, respectively. Since the electrical potentials of the two reference electrodes are essentially the same (i.e., $\Phi_{re1} \approx \Phi_{re2}$), Eq. (1) can be approximated by

$$V_{re1-re2} \approx \frac{1}{F}(\mu_{re1} - \mu_{re2}). \quad (2)$$

Further, the 4-electrode configuration is preferred for DC polarization measurements and is required for impedance measurements, as to be explained later.

2.3. Impedance spectroscopy

A computerized impedance analysis system, consisting of Solartron 1286 (electrochemical interface) and 1255 (frequency response analyzer), was used for impedance measurements. In impedance measurements, the generator of the measuring system applies stimuli (AC voltage) to the testing sample, and the analyzer of the system measures current response (phase shift and amplitude) of the sample while monitoring corresponding voltage [16]. In this study, the two cables carrying input signals (sinusoidal perturbations of a 10 mV amplitude, and DC bias if used) were connected to the two principal electrodes of the cell. The current response was also measured through the two same cables. The other two cables were for measuring the voltage response. Impedance spectra for different parts of the cell were acquired by varying connections of these two cables. In a conventional 2-probe impedance measurement, these two cables were also connected to the two principal electrodes and the obtained impedance represents the total impedance of the cell. If the interface of the cathode was to be studied, the two cables for measuring the voltage response were, respectively, connected to the cathode and a reference electrode of the same chemical potential. With this connection, the impedance of the half cell consisting of the cathode and a half of the electrolyte was measured, since the reference electrode always senses the potential at the symmetrical plane of the cell. Similarly, if the interface of the anode was to be studied, the two cables for measuring voltage response needed to be connected to the anode and a reference electrode of the same chemical potential, thus obtaining an impedance spectrum of the half cell consisting of the anode and a half of the electrolyte. It should be noted that, in order to obtain a correct half-cell impedance spectrum, the voltage response has to be measured between electrodes of equal chemical potential. Otherwise the difference in chemical potential would be superimposed to the voltage response, giving rise to an incorrect impedance spectrum. This is why it is necessary to use a 4-electrode configuration if the two sides of the electrolyte assume different chemical potentials.

In a Nyquist plot, the intercept of the impedance loop with the real axis at high frequencies corresponds to the resistance of the bulk electrolyte, R_b (under the assumption that the ohmic resistance of the silver leads is negligible), while the intercept of the impedance loop with the real axis at low frequencies corresponds to the total resistance of the cell, R_T. The polarization resistance of the electrode, R_p, can be calculated from these two measured parameters and the transference numbers of the electrolyte [25,29]. Impedance spectra measured in this study typically showed an inductive tail at high frequencies, which can be attributed to incomplete shielding of the silver leads in the furnace [30]. This artificial feature is not shown in the following impedance spectra.

2.4. Polarization measurements

The DC polarization measurements were made in either potentiostatic mode or galvanostatic mode using a Solartron 1286 and two millivoltmeters. The connections for measurements in both cases were essentially the same. Voltages between the two principal electrodes were applied (in potentiostatic mode) or measured (in galvanostatic mode) through two cables. Currents passing through the cell were measured or applied also through the same two cables. In the meantime, millivoltmeters were used to measure the voltages between either of the principal electrodes and a reference electrode, i.e. V_{ca-re} and V_{an-re}, where the suffixes ca, an, and re denote cathode, anode, and reference electrode, respectively. It is worth mentioning that while both the 3-electrode and the 4-electrode configurations can be used in the measurements, the 4-electrode configuration is more convenient for cells exposed to a gradient in chemical potential. Using a 4-probe cell, the half-cell voltage can be directly measured from the principal electrode and the reference electrode on the same side, without the inclusion of a chemical potential difference (otherwise the chemical potential difference needs to be subtracted from the measured voltage).

The measured V_{ca-re} (or V_{an-re}) contains two contributions: the interfacial overpotential, η_c (or η_a), and the ohmic drop of the electrolyte of the half-cell. The ohmic drop of the electrolyte can be determined from the measured current, ionic transference number of the electrolyte, and parameters obtained from impedance spectra. Thus the overpotentials of the cathode and the anode can be separated from the overall cell voltage. It should be noted that, in polarization measurements, sufficiently long time was allowed to take the steady-state readings, since the interfacial polarization was typically a slow relaxation process. In this study, more than 15 min may be needed to obtain steady-state currents and voltages under some conditions.

2.5. Confidence of the measurements

The essence of the 3-or 4-probe measurements is to separate one particular interface from the other interface in a solid-state device. The accuracy of such a separation is validated by the results of impedance measurements as shown in Fig. 3. In this case, impedance spectra were taken for a symmetrical cell at open cell conditions. This implies that the two principal electrodes would contribute equally to the total impedance. Fig. 3 shows that the impedance of each half-cell at any frequency is nearly half of the impedance for the full-cell at the corresponding frequency. In particular, the electrolyte resistance and the total resistance of each half-cell are both reduced by half as compared to those of the full cell. In addition, the sum of the impedance spectra of the two half-cells nearly duplicates the impedance spectrum of the full-cell. All these observations imply a successful separation of the performance of the two electrodes or interfaces. The slight difference between the impedance spectra of the two half-cells

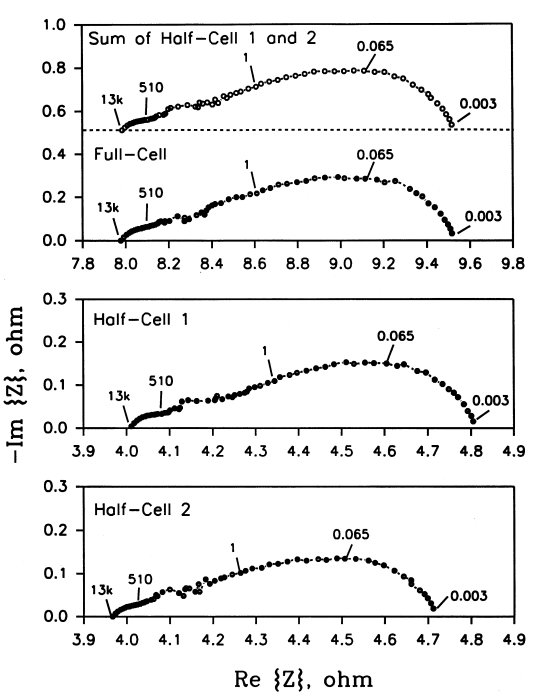

Fig. 3. Impedance spectra of the full-cell and the two half-cells of a Pt | BCG | Pt cell (relatively dense electrodes) measured at 800°C in air using a 3-electrode configuration. The sum of the impedance spectra of the two half-cells is also shown for comparison. Electrolyte thickness is 0.16 cm and electrode area is 0.385 cm^2. The numbers by data points are frequencies in Hz.

can be attributed to structural asymmetry between the electrodes or the electrolyte surfaces introduced during processing.

3. Applications

3.1. Identification of different processes

A major advantage of 3-or 4-probe impedance spectroscopy is that it isolates electrochemical characteristics of one electrode from another, and thus allows easy identification of processes occurring at different electrodes. This is particularly important for asymmetrical cells, in which the asymmetry may be caused by dissimilarities in electrode materials, chemical potential (atmosphere), or electrical potential (an applied voltage).

Shown in Fig. 4 are impedance spectra of a Pt | BCG | Pt cell at 722°C in argon, measured from the full-cell and the two half-cells, respectively. Comparison is being made for the impedance spectra with and without an applied DC bias. With a small DC bias (100 mV), the total polarization resistance of the interfaces increased significantly as compared to that without bias (Fig. 4(a)). However, not much information can be readily extracted from the impedance spectra measured from the full cell with respect to the cause of this change. The impedance spectra measured from the two half-cells tell much more. The significant increase in the total polarization resistance upon applying a DC bias seems to originate from significant concentration polarization of oxygen at the cathode, due to the limitation of mass transfer to the electrolyte–electrode interface (Fig. 4(c)) [25]. The polarization resistance of the anode, in fact, decreased with the amplitude of the bias as compared to that without bias, due perhaps to an enhancement of charge transfer by the applied electric field (Fig. 4(b)) [30].

Shown in Fig. 5 is another example of identification of different processes by 4-probe impedance spectroscopy. The impedance spectra of the same Pt | BCG | Pt cell measured in air were compared to those measured under a fuel cell condition (H_2 + 3%H_2O, Pt | BCG | Pt, air) at the same temperature (722°C). From the total impedance spectra measured

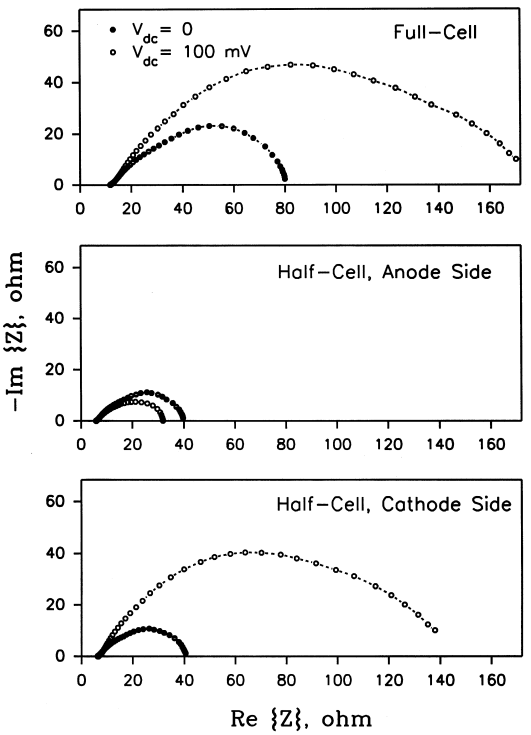

Fig. 4. Comparison of impedance spectra, measured at 722°C in Ar, of a Pt | BCG | Pt cell (porous electrodes) with and without DC bias. Electrolyte thickness is 0.09 cm, and electrode area is 0.385 cm^2.

from the full-cell as shown in Fig. 5(a), it is clear that both electrolyte resistance and total resistance of the cell were greater when measured under the fuel cell condition than those measured in air. Apparently, these differences should be a consequence of the changes in resistance of the anode side, since the only apparent difference between the two situations was the atmosphere on the anode side. However, this turns out to be incorrect. The impedance spectra of the two half-cells shown in Fig. 5(b) and (c) indicate that, upon changing the cell environment from a symmetrical atmosphere (air) to the fuel cell condition, the resistances of both anode and cathode sides changed. This can be explained as follows. First, the BCG electrolyte is an MIEC when immersed in air and becomes a nearly pure ionic conductor under fuel cell conditions [25]. The dis-

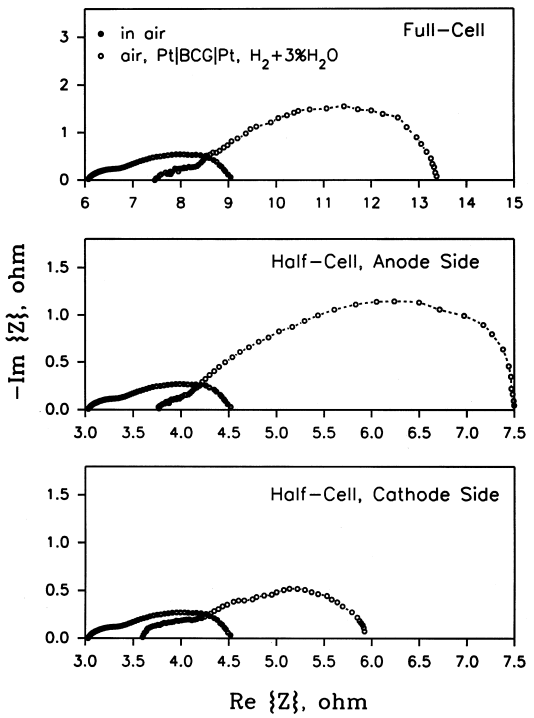

Fig. 5. Comparison of impedance spectra of a Pt | BCG | Pt cell measured in air and under a fuel cell condition (H_2 + 3%H_2O,Pt | BCG | Pt,air) at the same temperature (722°C), using the same sample as in Fig. 4.

appearance of electronic conduction under the fuel cell condition results in an increase in electrolyte resistance. Second, the anodic interfacial resistance of the cell changed significantly when the cell was switched from immersion in air to the fuel cell conditions, because the species involved in the anodic reactions are completely different. Third, the interfacial resistance of the cathode in air appears to be smaller as compared to that under fuel cell conditions, since the electronic conduction in the former case partially short-circuits the ionic conduction [29]. Finally, the BCG electrolyte is conductive to both oxygen ion and proton, and thus water evolution takes place on both cathode and anode of the fuel cell. Water evolution, however, hinders the cathodic kinetics and enhances the anodic kinetics of a fuel cell based on a BCG electrolyte [25]. This is another cause for the increase of cathodic resistance.

3.2. Determination of electrode kinetic parameters by impedance spectroscopy under open cell conditions

As mentioned earlier, the electrolyte resistance, R_b, and the total resistance of the cell, R_T, can be readily determined from the intercepts of the impedance loop with the real axis. Consequently, the polarization resistance of the electrode, R_p, can be calculated from the measured parameters. Shown in Fig. 6 is a simplified equivalent circuit representation of a solid-state electrochemical cell based on an electrolyte of MIECs, where R_i and R_e are the ionic and electronic resistances of the electrolyte, respectively, and C_p is the capacitance of the interface due to polarization [31]. R_b and R_T are related to R_i, R_e, and R_p as follows:

$$R_b = \frac{R_i R_e}{R_i + R_e}, \tag{3}$$

$$R_T = \frac{(R_i + R_p)R_e}{(R_i + R_p) + R_e}. \tag{4}$$

On the other hand, the ionic transference number of the electrolyte can be expressed as

$$t_i = \frac{R_e}{R_i + R_e}. \tag{5}$$

Solving for R_p from Eqs. (3)–(5), we have

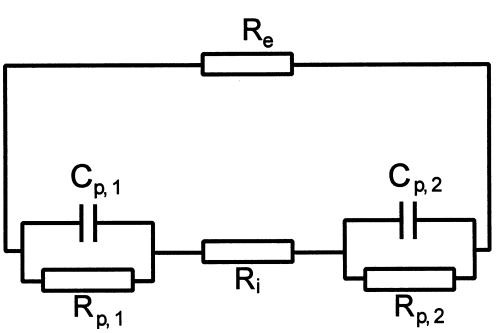

Fig. 6. Simplified equivalent circuit of a solid-state cell based on an electrolyte of MIECs.

$$R_p = \frac{R_b(R_T - R_b)}{t_i[t_i R_T - (R_T - R_b)]}. \quad (6)$$

In this case, the ionic transference number needs to be determined by other measurements [25]. In particular, if $t_i = 1$, Eq. (6) reduces to

$$R_p = R_T - R_b \quad (7)$$

which gives R_p for a cell with an electrolyte of a pure ionic conductor.

The above equations can be used for both full-cell and half-cell. If R_b and R_T are determined from impedance spectra of a full-cell, then the calculated R_p is the total polarization resistance of the two electrolyte–electrode interfaces. If R_b and R_T are determined from impedance spectra of a half-cell, the calculated R_p is the polarization resistance of a single electrolyte–electrode interface. For symmetrical cells, it can be assumed that the two interfaces contribute equally to the total impedance, thus the polarization resistance of each electrode can be determined from impedance spectra of the full-cell measured in 2-probe configuration. In order to determine the polarization resistance of different electrodes of an asymmetrical cell, one has to use 3- or 4-probe impedance spectroscopy to measure the impedance spectrum of each half-cell.

The amplitude of an AC perturbation used in impedance measurements is usually sufficiently small (10 mV in this study). When the steady-state current passing through the cell is also sufficiently small, as in the case of open cell conditions, the obtained R_p is directly related to the charge transfer resistance, R_{ct}, or the mass transfer resistance, R_{mt}, or the combination of these two. Shown in Fig. 7 are R_p as a function of temperature measured in air without DC bias for a Pt | BY | Pt cell and a Pt | BCG | Pt cell. The R_p data in the case of Pt | BY | Pt cell were calculated from R_b and R_T as determined from 2-probe impedance spectroscopy using Eq. (7), since BY is a nearly-pure oxygen ion conductor. The magnitudes of R_p are in good agreement with the results reported for Er-stabilized Bi_2O_3 electrolytes with sputtered Pt electrodes [32]. The R_p data in the case of Pt | BCG | Pt cell were calculated from R_b and R_T (as determined from 2-probe impedance spectroscopy) and ionic transference numbers of the BCG electrolyte (ranging from 0.57 to 0.63 depending on temperature, determined under similar conditions [25]) using Eq. (6), noting that BCG is an MIEC under the testing conditions. The plot of $\log(1/R_p)$ versus $1/T$ in both cases shows a linear relation. The activation energy for the electrode kinetics was determined to be 2.1 eV for the Pt | BY | Pt cell and 1.2 eV for the Pt | BCG | Pt cell, respectively.

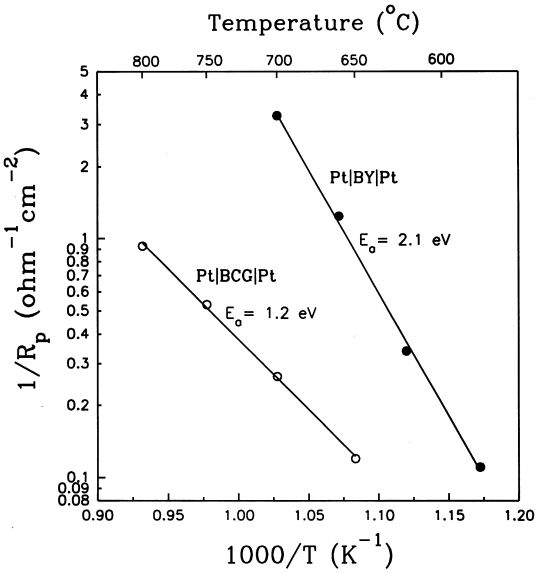

Fig. 7. Interfacial polarization resistance, R_p, measured in air for a Pt | BY | Pt cell and a Pt | BCG | Pt cell as a function of temperature.

Shown in Fig. 8 are electrode polarization resistance as a function of partial pressure of oxygen (P_{O_2}) for a Pt | BY | Pt cell and a Pt | BCG | Pt cell measured at 722°C under open cell conditions. Again, the R_p data in the case of Pt | BY | Pt cell were calculated from R_b and R_T values using Eq. (7), and the R_p data in the case of Pt | BCG | Pt cell were calculated from R_b and R_T values and ionic transference numbers of the BCG electrolyte determined under similar conditions (ranging from 0.54 at P_{O_2} = 1 atm to 0.97 at $P_{O_2} = 5\times10^{-5}$ atm) [25] using Eq. (6). In the P_{O_2} range studied (5×10^{-5} to 1 atm), the Pt | BY | Pt cell showed a single linear relation between $\log(1/R_p)$ and $\log(P_{O_2})$, with a slope of about 0.29. This slope, being close to 1/4, suggests that charge transfer is the rate-limiting step in the

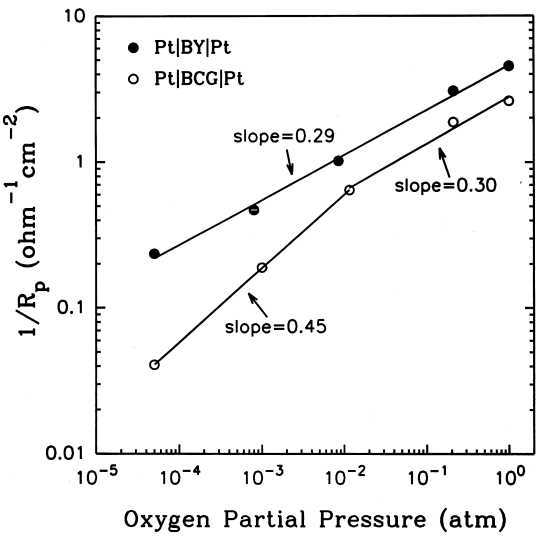

Fig. 8. Interfacial polarization resistance, R_p, measured at 722°C for a Pt | BY | Pt cell and a Pt | BCG | Pt cell as a function of partial pressure of oxygen.

oxygen reduction and evolution process [6,33,34]. The Pt | BCG | Pt cell, on the other hand, showed two segments of the linear relation between $\log(1/R_p)$ and $\log(P_{O_2})$. The segment at high oxygen partial pressures showed a slope of about 0.30, while the segment at low oxygen partial pressures showed a slope of about 0.45, suggesting that the rate-limiting mechanism is different in different ranges of oxygen partial pressures. Charge transfer seemed to be rate-limiting only at high oxygen partial pressures. At low oxygen partial pressures, mass transfer became the rate-limiting step, as evidenced by the slope of $\log(1/R_p)$ versus $\log(P_{O_2})$ being close to 1/2 [3,6,33]. This is consistent with the observation of significant concentration polarization for the cathode of the Pt | BCG | Pt cell at low oxygen partial pressures (see Fig. 4).

3.3. Determination of electrode kinetic parameters by impedance spectroscopy with DC bias

Under an applied DC bias, there is an appreciable steady-state current passing through the cell, and thus R_p is no longer equivalent to R_{ct} or R_{mt} or their combination. The total polarization resistance of the cell, which is the sum of the polarization resistances of the two individual electrodes, may change in either direction with the amplitude of an applied DC bias, depending on the nature of the rate-limiting step of the interfacial processes. In general, an increase in R_p with the amplitude of a DC bias signifies concentration polarization at the interfaces (in either the gas or the solid phase, or both), thus indicating that mass transfer is rate-limiting [25,34], as we have seen earlier in Fig. 4. In contrast, a decrease in R_p with the amplitude of a DC bias is usually an evidence of field-enhancement of charge transfer processes, thus suggesting that charge transfer is rate-limiting [30,35]. The individual polarization resistances, however, may change in the same direction or in the opposite directions depending on different situations.

Fig. 9 shows a series of impedance spectra of a Pt | BY | Pt cell measured at 700°C in air under different amplitudes of applied DC biases. The total polarization resistance decreased with the amplitude of the DC bias (Fig. 9(a)). The polarization resistances of the cathode ($R_{p,c}$) and the anode ($R_{p,a}$)

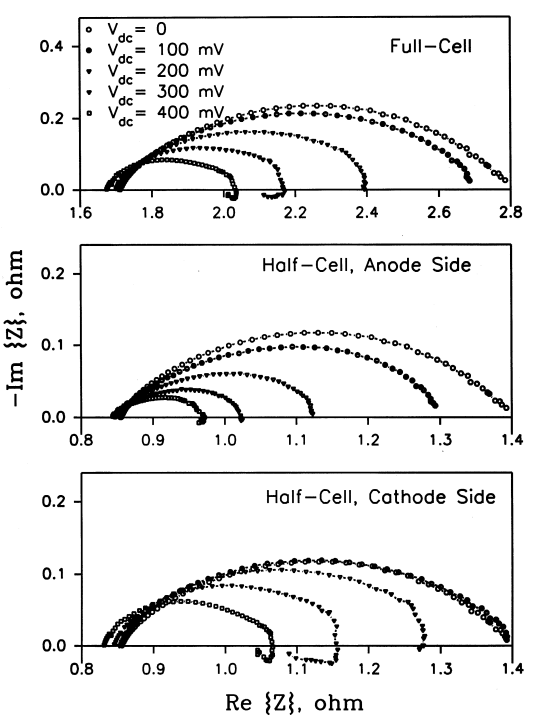

Fig. 9. Impedance spectra of a Pt | BY | Pt cell measured at 700°C in air under different amplitudes of applied DC bias. Electrolyte thickness is 0.07 cm, and electrode area is 0.385 cm^2.

both changed in the same direction. Accordingly, charge transfer seems to be the rate-limiting step in this case, and this is consistent with the conclusion drawn from the dependence of R_p on P_{O_2} shown earlier (Fig. 8). Furthermore, when the applied DC bias is higher than 300 mV, impedance spectra with an inductive feature at low frequencies were observed for both the anode and the cathode. This observation is viewed as an evidence of significant enhancement of the electrode reactions [30,35].

Fig. 10 shows a series of impedance spectra of a Pt | BCG | Pt cell measured at 800°C in air under different amplitudes of applied DC biases. The total polarization resistance decreased slightly with the amplitude of the DC bias (Fig. 10(a)). However, the cathode resistance changed in the opposite direction. While the anode resistance decreased significantly with the amplitude of an applied DC bias (Fig. 10(b)), the cathode resistance increased slightly with the amplitude of DC bias (Fig. 10(c)). In this case, the overall electrode reactions seems to be limited by

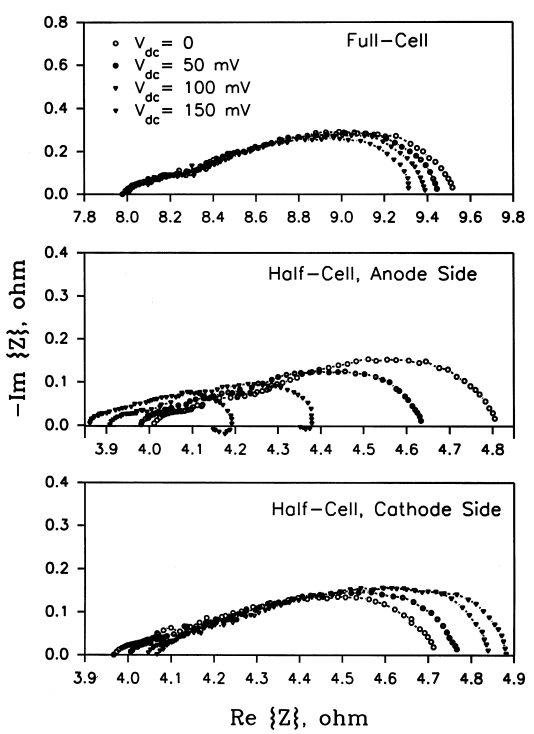

Fig. 10. Impedance spectra of a Pt | BCG | Pt cell measured at 800°C in air under different amplitudes of DC bias. Electrolyte thickness is 0.16 cm, and electrode area is 0.385 cm^2.

charge transfer, being consistent with the conclusion based on the dependence of R_p on P_{O_2} shown earlier (Fig. 8). However, upon applying a DC bias, the concentration polarization due to mass transfer became significant at cathode, while charge transfer process was significantly enhanced at anode. Another important feature to note is that the applied bias also induced appreciable shifts in the electrolyte resistance of both half-cells. This may be explained as follows. A gradient in oxygen partial pressure was present across the electrolyte when a DC bias was applied. This in turn resulted in a gradient in the electronic conductivity, since the electronic conductivity of the BCG electrolyte (p-type) was found to increase with increasing oxygen partial pressure [25]. Increasing the amplitude of a DC bias resulted in an increase in oxygen partial pressure in the electrolyte on the anode side (due to the positive polarity) and a decrease in oxygen partial pressure in the electrolyte on the cathode side (due to the negative polarity). Consequently, with increasing DC bias, the R_b of the anodic half-cell decreased as the electronic conductivity of the electrolyte on the anode side increased, and the R_b of the cathodic half-cell increased as the electronic conductivity of the electrolyte on the cathode side decreased. On the other hand, the R_b of the full-cell did not change with the amplitude of DC bias; this indicates that the average electronic conductivity of the whole electrolyte remained nearly constant.

The individual polarization resistances measured under the influence of an applied DC bias are related to cathodic overpotentials (η_c) and anodic overpotentials (η_a) as follows:

$$\eta_c = I_i R_{p,c}, \tag{8}$$

$$\eta_a = I_i R_{p,a}, \tag{9}$$

where I_i is the steady-state DC ionic current passing through the cell. For a cell based on an MIEC electrolyte, I_i can be determined as follows (see Fig. 6):

$$I_i = I - I_e = \frac{V}{R_T} - \frac{V}{R_e} \tag{10}$$

where V is the applied DC bias across the full cell, R_T is the total resistance of the full cell, and R_e is the

electronic resistance of the whole electrolyte. In view of Eqs. (3) and (5), Eq. (10) can be rewritten as

$$I_i = V\left(\frac{1}{R_T} - \frac{1-t_i}{R_b}\right). \quad (11)$$

The $R_{p,c}$ and $R_{p,a}$ in Eqs. (8) and (9) can be calculated using Eq. (6) provided that all parameters in Eq. (6), R_T, R_b, and t_i, are determined from the corresponding half-cells. Due to the shifts in electrolyte resistance of the half-cells, the ionic transference numbers used for the calculation should be corrected for each bias. Noting $R_b = t_i R_i$ and assuming R_i is independent of oxygen partial pressure (and thus DC bias), we have

$$t_i = \frac{R_b}{R_{b,o}} t_{i,o} \quad (12)$$

where $R_{b,o}$ and $t_{i,o}$ denote, respectively, the electrolyte resistance and the ionic transference number at zero bias under open cell conditions.

For cells based on electrolytes of a pure ionic conductor, Eqs. (8) and (9) and (11) reduce, respectively, to

$$\eta_c = IR_{p,c}, \quad (13)$$

$$\eta_a = IR_{p,a}, \quad (14)$$

$$I = \frac{V}{R_T}, \quad (15)$$

where I is the observed or total DC current passing through the cell whereas $R_{p,c}$ and $R_{p,a}$ can be determined from impedance spectra of half-cells using Eq. (7).

The changes in polarization resistance with the amplitude of DC bias can be expressed as its dependence on the interfacial overpotential. Shown in Fig. 11 are changes in polarization resistance with DC bias for the Pt | BY | Pt cell under the same conditions as for Fig. 9, and for the Pt | BCG | Pt cell under the same conditions as for Fig. 10. The different $R_{p,c} - \eta_c$ dependencies for the two cells again reflect different rate-limiting mechanisms of the cathodic reactions in the two cases.

Further, current–overpotential curves can be plotted, as shown in Fig. 12 for the Pt | BY | Pt cell. If similar measurements are extended to a wider range of applied DC biases, linear plots of current–overpotential can be constructed at low DC biases and Tafel plots may be constructed at higher DC biases, from which the exchange current density,

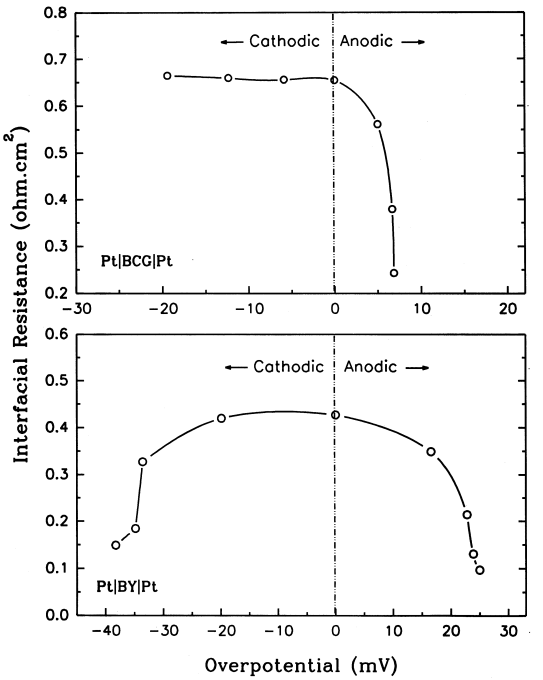

Fig. 11. Changes in polarization resistance with the amplitude of an applied DC bias for the same Pt | BY | Pt cell and under the same conditions as in Fig. 9, and for the same Pt | BCG | Pt cell and under the same conditions as in Fig. 10.

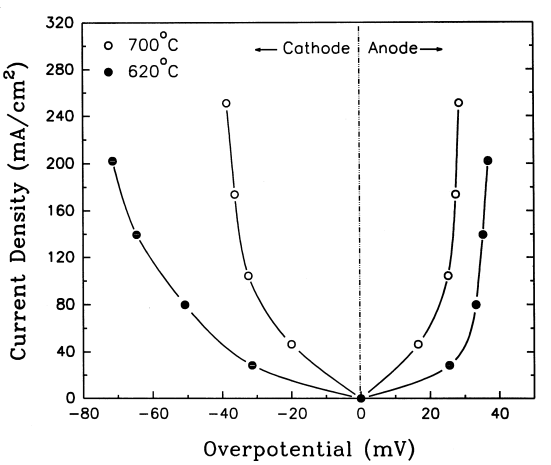

Fig. 12. Current–overpotential curves for the same Pt | BY | Pt cell under the same conditions as in Fig. 9.

mass transfer limited current density, as well as the cathodic and anodic transfer coefficients (α_c and α_a) may be determined [15].

3.4. Determination of electrode kinetic parameters by polarization measurements

As mentioned earlier, both V_{ca-re} and V_{an-re} are measured in polarization measurements. Since each of them contains two terms: the interfacial overpotential, η_c (or η_a), and the ohmic drop of the electrolyte of the half-cell, the cathodic and anodic overpotentials can be determined as follows for a cell with mixed conducting electrolyte:

$$I_i = I - \frac{V}{R_e} = I - \frac{V(1-t_i)}{R_b}, \tag{16}$$

$$\eta_c = V_{ca-re} - \frac{1}{2} I_i R_i = V_{ca-re} - \frac{I_i R_{b,o}}{2t_{i,o}}, \tag{17}$$

$$\eta_a = V_{an-re} - \frac{1}{2} I_i R_i = V_{an-re} - \frac{I_i R_{b,o}}{2t_{i,o}}, \tag{18}$$

where I_i is the ionic current passing through the cell, I is the total current passing through the cell (measured or applied), V is the voltage across the full-cell (applied or measured), R_b, $R_{b,o}$, t_i, and $t_{i,o}$ are the same as defined for Eq. (12), while R_b and $R_{b,o}$ here are measured from the full cell. It should be noted that although the DC bias may induce a shift in the R_b of each half-cell, the shift has little effect on the determination of η_c and η_a from polarization measurements, since R_i is nearly constant ($=R_{b,o}/t_{i,o}$), and the R_b and the average t_i of the full-cell are also nearly constant, as seen earlier.

For cells based on electrolytes of a pure ionic conductor, $I_i = I$, $R_i = R_b$, and $t_i = 1$; thus Eqs. (17) and (18) reduce, respectively, to

$$\eta_c = V_{ca-re} - \frac{1}{2} I R_b, \tag{19}$$

$$\eta_c = V_{ca-re} - \frac{1}{2} I R_b. \tag{20}$$

Shown in Fig. 13 are Tafel plots of a Pt | BY | Pt cell at 580°C in air constructed from polarization data (V_{ca-re} and V_{an-re}) measured on a 3-electrode cell and from R_b values determined from impedance spectra. Tafel behavior was observed for both cathode and anode over a wide range of overpotentials. The exchange current density was obtained directly from either of the extrapolated intercepts at $\eta = 0$ of the Tafel plots. The intercepts (at $\eta = 0$) from the plots of both cathodic and anodic direction are very close (6.7 mA cm^{-2} and 6.4 mA cm^{-2}, respectively). The cathodic transfer coefficient, α_c, was calculated to be about 1.0 from the Tafel slope in the cathodic direction. Similarly, the anodic transfer coefficient, α_a, was calculated to be about 1.1 from the Tafel slope. Further, the stoichiometric coefficient can be determined as [15]

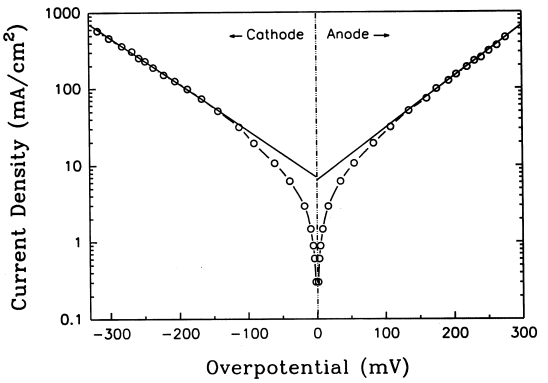

Fig. 13. Tafel plots of a Pt | BY | Pt cell at 580°C in air constructed from polarization data of 3-electrode cell and from the R_b values from impedance spectra.

$$\nu = n/(\alpha_c + \alpha_a) \tag{21}$$

where n is the total number of electrons involved in the overall reaction.

Current–overpotential relations at low overpotentials yielded a linear plot, as shown in Fig. 14 for the same Pt | BY | Pt cell under the same conditions as for Fig. 13. The exchange current density was calculated to be 6.2 mA cm^{-2} from the data for the cathodic direction and 6.3 mA cm^{-2} from the data for the anodic direction. It has been shown that the assessments of the exchange current density using different methods based on polarization measurements yielded similar values, in the vicinity of 6.4 mA cm^{-2}. These results are also consistent with the results from the impedance spectroscopy (shown in Fig. 7).

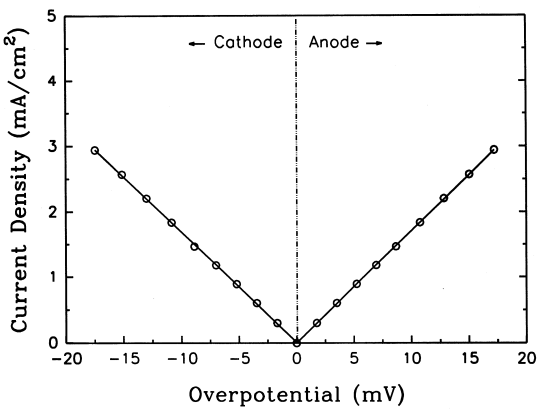

Fig. 14. Linear plot of current–overpotential relations at low overpotentials for the same Pt | BY | Pt cell and under the same conditions as in Fig. 13.

4. Conclusions

The application of 3-probe or 4-probe impedance and polarization measurements to interfacial studies of solid-state electrochemical cells has been elaborated. These techniques can be consistently applied to cells based on electrolytes of pure ionic conductors and cells based on electrolytes of mixed ionic–electronic conductors (MIECs). Combination of these techniques offers an effective approach to studies of electrode kinetics and transport properties of each cell component. The uniqueness of these techniques include separating the response of each cell component, measuring the interfacial polarization resistances and overpotentials of each individual interface, identifying reaction mechanisms (the nature of rate-limiting steps), and determining various kinetic parameters. Several applications of these techniques are illustrated in characterization of two representative cells ($Pt \mid BaCe_{0.8}Gd_{0.2}O_3 \mid Pt$ and $Pt \mid Bi_{1.5}Y_{0.5}O_3 \mid Pt$) under different conditions.

5. Notation

List of symbols

μ_{re1}, μ_{re2}	chemical potential of electrons at the surface of the MIEC electrolyte in contact with the two reference electrodes (re1 and re2), J mol^{-1}
Φ_{re1}, Φ_{re2}	electrical potential of the two reference electrodes (re1 and re2), V
F	Faraday's constant, 96 487 C eq^{-1}
V	total voltage across the cell, V
V_{an-re}	voltage between the anode and a reference electrode, V
V_{ca-re}	voltage between the cathode and a reference electrode, V
$V_{re1-re2}$	voltage across the two reference electrodes (re1 and re2), V
η_a, η_c	anodic and cathodic overpotential, respectively, V
R_b	resistance of the electrolyte, Ω cm^2
$R_{b,o}$	resistance of the electrolyte under open cell conditions, Ω cm^2
R_p	interfacial polarization resistance, Ω cm^2
R_T	total resistance of the cell, Ω cm^2
R_i, R_e	ionic and electronic resistance of the electrolyte, respectively, Ω cm^2
R_{ct}, R_{mt}	resistance to charge transfer and mass transfer, respectively, Ω cm^2
$R_{p,a}$, $R_{p,c}$	interfacial polarization resistance at the anode and the cathode, respectively, Ω cm^2
C_p	interfacial polarization capacitance, F cm^{-2}
t_i	ionic transference number, dimensionless
$t_{i,o}$	ionic transference number under open cell conditions, dimensionless
T	absolute temperature, K
P_{O_2}	partial pressure of oxygen, atm
I	total current, A
I_i	ionic current, A
I_e	electronic current, A
α_a, α_c	anodic and cathodic transfer coefficient, respectively, dimensionless
ν	stoichiometric coefficient of the species in electrode reaction, dimensionless
n	total number of electrons exchanged in electrode reaction

Subscripts

ca	cathode

an	anode
re1	reference electrode 1
re2	reference electrode 2
re	reference electrode
i	ionic
e	electronic
ct	charge transfer
mt	mass transfer

Abbreviations

SOFC	solid oxide fuel cell
MIEC	mixed ionic–electronic conductor
BCG	gadolinium-doped barium cerate ($BaCe_{0.8}Gd_{0.2}O_3$)
BY	yttria-stabilized bismuth oxide ($Bi_{1.5}Y_{0.5}O_3$)

Acknowledgements

This work was supported by NSF under award No. DMR-9357520 and EPRI under contract No. RP1676-19 and their financial support of this research is greatly appreciated.

References

[1] E.C. Subbarao, H.S. Maiti, Solid State Ionics 11 (1984) 317.
[2] A.J. Burggraaf, M.P. Van Dijk, K.J. De Vries, Solid State Ionics 18–19 (1986) 807.
[3] Y. Takeda, R. Kanno, M. Noda, Y. Tomida, O. Yamamoto, J. Electrochem. Soc. 134 (1987) 2656.
[4] S. Liou, W.L. Worrell, in: S.C. Singhal (Ed.), Proceedings of 1st International Symposium on SOFC, PV 89-11, The Electrochemical Society Proceedings Series, Pennington, NJ, 1989, p. 81.
[5] M. Liu, in: T.A. Ramanarayanan, H.L. Tuller (Ed.), Proceedings of 1st International Symposium on Ionics and Mixed Conducting Ceramics, PV 91-12, The Electrochemical Society Proceedings Series, Pennington, NJ 1991, p. 191.
[6] M. Liu, A. Khandkar, Solid State Ionics 52 (1992) 3.
[7] M. Suzuki, H. Sasaki, S. Otoshi, A. Kajimura, N. Sugiura, M. Ippommatsu, J. Electrochem. Soc. 141 (1994) 1928.
[8] M. Watanabe, H. Uchida, M. Shibata, N. Mochizuki, K. Amikura, J. Electrochem. Soc. 141 (1994) 342.
[9] K.R. Thampi, A.J. McEvoy, J. Van herle, J. Electrochem. Soc. 142 (1995) 506.
[10] T. Ishihara, T. Kudo, H. Matsuda, Y. Takita, J. Electrochem. Soc. 142 (1995) 1519.
[11] A.J.A. Winnubst, A.H.A. Scharenbory, A.J. Burggraaf, J. Appl. Electrochem. 15 (1985) 139.
[12] G.B. Barbi, C.M. Mari, Solid State Ionics 6 (1982) 341.
[13] J.M. Azad, S. Larose, S.A. Akbar, J. Mater. Sci. 29 (1994) 4135.
[14] J.S. Newman, Electrochemical Systems, 2nd ed., Prentice Hall, Englewood Cliffs, NJ, 1991.
[15] A.J. Bard, L.R. Faulkner, Electrochemical Methods, Fundamentals and Applications, Wiley, New York, 1980.
[16] J.R. Macdonald, Impedance Spectroscopy, Wiley, New York, 1987.
[17] D.Y. Wang, A.S. Nowick, J. Electrochem. Soc. 126 (1979) 1155.
[18] B.A. Boukamp, I.C. Vinke, K. Seshan, K.J. De Vries, A.J. Burggraaf, Solid State Ionics 28–30 (1988) 1187.
[19] M. Liu, S.J. Visco, L.C. De Jonghe, Electrochimica Acta 38 (1993) 1289.
[20] R.D. Armstrong, M. Todd, in: P.G. Bruce (Ed.), Solid State Electrochemistry, Cambridge University Press, Cambridge, 1995, p. 264.
[21] N. Bonanos, B. Ellis, K.S. Knight, M.N. Mahmood, Solid State Ionics 35 (1989) 179.
[22] N. Taniguchi, K. Hatoh, J. Niikura, T. Gamo, H. Iwahara, Solid State Ionics 53–56(2) (1993) 998.
[23] D. Stevenson, N. Jiang, R. Buchanan, F. Henn, Solid State Ionics 62 (1993) 279.
[24] K.D. Kreuer, E. Schonherr, J. Maler, Solid State Ionics 70–71 (1994) 278.
[25] M. Liu, H. Hu, W. Rauch, in: H. Anderson, A. Khandkar, M. Liu (Ed.), Proceedings of 1st International Symposium on Ceramic Membranes, PV 95-24, The Electrochemical Society, Pennington, NJ, 1996, p. 192.
[26] T. Takahashi, H. Iwahara, T. Arao, J. Appl. Electrochem. 5 (1975) 187.
[27] C. Wang, X. Xu, B. Li, Solid State Ionics 13 (1984) 135.
[28] W. Rauch, M. Liu, J. Electrochem. Soc. 144 (1997) 4049.
[29] M. Liu, H. Hu, J. Electrochem. Soc. 143 (1996) L109.
[30] B. Gharbage, T. Pagnier, A. Hammou, J. Electrochem. Soc. 141 (1994) 2118.
[31] M. Liu, A. Joshi, in: T.A. Ramanarayanan, H.L. Tuller, (Ed.), Proceedings of 1st International Symposium on Ionics and Mixed Conducting Ceramics, PV 91-12, The Electrochemical Society Proceedings Series, Pennington, NJ, 1991, p. 231.
[32] I.C. Vinke, J.L. Bakiewicz, B.A. Boukamp, K.J. De Vries, A.J. Burggraaf, Solid State Ionics 40–41 (1990) 886.
[33] O. Jacob Velle, T. Norby, Solid State Ionics 52 (1992) 93.
[34] S.F. Chehab, J.D. Canaday, A.K. Kuriakose, A. Ahmad, T.A. Wheat, P.G. Komotowski, Solid State Ionics 59 (1993) 125.
[35] E.J.L. Schouler, M. Kleitz, J. Electrochem. Soc. 134 (1987) 1045.